Møller-Plesset and density-fixed adiabatic connections for a model diatomic system at different correlation regimes

Sara Giarrusso[1, a)] and Aurora Pribram-Jones[1, b)]
Department of Chemistry and Biochemistry, University of California Merced, 5200 North Lake Rd. Merced, CA 95343, USA

(Dated: 17 May 2023)

In recent years, Adiabatic Connection Interpolations developed within Density Functional Theory (DFT) have been found to provide satisfactory performances in the calculation of interaction energies when used with Hartree-Fock (HF) ingredients. The physical and mathematical reasons for such unanticipated performance have been clarified, to some extent, by studying the strong-interaction limit of the Møller-Plesset (MP) adiabatic connection. In this work, we calculate both the MP and the DFT adiabatic connection (AC) integrand for the asymmetric Hubbard dimer, which allows for a systematic investigation at different correlation regimes by varying two simple parameters in the Hamiltonian: the external potential, Δv, and the interaction strength, U. Noticeably, we find that, while the DFT AC integrand appears to be convex in the full parameter space, the MP integrand may change curvature twice. Furthermore, we discuss different aspects of the second-order expansion of the correlation energy in each adiabatic connection and we demonstrate that the derivative of the λ-dependent density in the MP adiabatic connection at $\lambda = 0$ (i.e., at the HF density) is zero. Concerning the strong-interaction limit of both adiabatic connections, we show that while, for a given density, the asymptotic value of the MP adiabatic connection, W_∞^{HF}, is lower (or equal) than its DFT analogue, W_∞^{KS}, this is not always the case for a given external potential.

I. INTRODUCTION AND THEORETICAL BACKGROUND

Adiabatic connection methods rely on the idea of gradually switching from a formally non-interacting Hamiltonian, which is comparatively simple, to a "fully interacting" one, which is more complicated and describes the actual electronic system of interest. This is done by multiplying the interaction operator by a coupling- or interaction-strength parameter.

Nowadays, there are several different flavors of adiabatic connections adopted in wavefunction-based methods;[1–10]however, the formalism was first developed in the context of Density Functional Theory (DFT)[11–13] and it has been a quite powerful tool to construct models for the exchange-correlation (XC) energy in Kohn-Sham DFT[14] ever since. Indeed, it has provided the rationale for density functional approximations (DFAs) such as hybrid,[15,16] double-hybrid,[17] and functionals from the random phase approximation,[18] all of which encode the exact behaviour of the adiabatic connection at small coupling, where the interaction can be treated as a perturbation.

In addition to these types of functionals however, this formalism has also inspired the construction of DFAs that interpolate between two different limits of the adiabatic connection curve, performing what is effectively an (approximate) all-order resummation of the perturbation series. Initially, DFAs of this kind were built as an interpolation between the zero- and the full-interaction limits,[19] but, shortly afterwards, more balanced interpolations were constructed by extending the range of the coupling strength *beyond* the physical value, bringing it to infinity[20–24] and thus combining the information coming from equally extreme limits (where equally extreme is in the sense that the coupling-strength parameter λ in front of the interaction operator in the two limits behaves as $\lambda \to \infty$ or $\alpha \to \infty$ with $\alpha = \frac{1}{\lambda}$). This class of DFAs, collectively referred to as Adiabatic Connection (Interaction) Interpolations (ACIIs or ACIs) or Adiabatic Connection Methods (ACMs), has recently drawn much attention. One important reason for such renewed interest is that their lack of size-consistency can be corrected very easily at no extra computational cost, as shown in Ref. 25. Another fundamental reason is that, although having been originally devised in a DFT framework, ACMs have been shown to provide satisfactory performances for binding and interaction energies (in non-covalent complexes), when used with Hartree-Fock (HF) ingredients.[25–28]

Their use in this framework has numerous practical advantages compared to their use in KS-DFT and some theoretical downsides. The downside compared to KS-DFT is that ACMs on HF ingredients are a simple energetic correction to the HF approximation: they cannot be used to obtain the interacting density via a self-consistent-field (SCF) scheme. On the contrary, ACMs within KS-DFT can in principle yield an approximate interacting density via an SCF calculation, but with the practical disadvantage that their implementation is quite involved and expensive, due to the presence of functional derivatives.[29,30] Indeed, ACMs within DFT have been mostly used on approximate KS orbitals, obtained from a preceding SCF calculation, but this strategy introduces an extra layer of approximation, falls back into the known problem of having to "cherry-pick" the best functional for the calculation at hand, and seems to be overall not quite accurate.[26]

By contrast, when using ACMs within the MP adiabatic

[a)] Electronic mail: sgiarrusso@ucmerced.edu
[b)] Electronic mail: apj@ucmerced.edu

connection, the orbitals required from the theory are simply the HF orbitals, which are fixed once for all in the initial HF calculation. This use of interpolation formulas with the HF density and orbitals has been theoretically supported by studies on the strong-interaction limit of the associated adiabatic connection[31,32] (see also Ref. 33 for a review).

Although these theoretical advancements pave the way for the use of HF ingredients in a density-functional spirit, many things still need to be better understood. For instance, the ACMs were constructed as convex interpolants, since the DFT adiabatic connection is reckoned to be (piecewise) convex. However, the MP adiabatic connection is known to be concave in the small-interaction region for some simple atomic and molecular systems,[4,27,34] therefore some variations of ACMs had to be developed to accommodate this feature.[28] To further the development of ACMs in both frameworks, we present in this work a careful comparison between the MP and the DFT adiabatic connection for a model diatomic system at different correlation regimes: the asymmetric Hubbard dimer. This model has been useful in the context of Site-Occupation Function Theory (SOFT), the analogue of DFT for lattice systems, because the density (or "site-occupation difference" in the model) can be varied easily by varying two simple parameters in the model Hamiltonian.

In the following, we review the theory of the MP and DFT adiabatic connections (section I A) as well as the model system (section I B). Section II translates the two adiabatic connections in the language of the Hubbard dimer, while section III illustrates the results of the calculations: the shapes of the two curves at different points in the parameter space (section III A), the performance of a proposed indicator[27] as a predictor of the accuracy of the correlation energy expanded up to second-order (section III B) and the density as a function of the coupling parameter in the MP adiabatic connection (section III C). Section IV focuses entirely on the strong-interaction limit of the two adibatic connections, while section V gives some conclusive remarks.

A. Møller-Plesset and density-fixed adiabatic connections

Let us start from the usual non-relativistic electronic Hamiltonian

$$\hat{H} = \hat{T} + \hat{V}_{ee} + \hat{V}, \tag{1}$$

with $\hat{T} = -\sum_i^N \frac{\nabla_i^2}{2}$ the kinetic energy, N the number of particles in the system, $\hat{V}_{ee}$ the Coulomb interaction between all electron pairs, and $\hat{V} = \sum_i^N v(i)$ the N-particle sum of the external potential, (typically) given by the positive field of the nuclei, felt by each electron. The lowest (ground) eigenstate associated with this Hamiltonian is labelled Ψ. According to the Hartree-Fock approximation, the expectation value of $\hat{H}$ is minimized in the space of Slater determinants. Slater determinants are defined as $\Phi := \sum_P (-1)^P \psi_{P(1)}(\mathbf{x}_1)\cdots\psi_{P(N)}(\mathbf{x}_N)$, where the $\psi_n(\mathbf{x})$ are single-particle wave functions, spatial and spin coordinates are considered separable, i.e. $\psi_n(\mathbf{x}) \equiv \phi_n(\mathbf{r})s_n(\sigma)$, and the index P lists all possible permutations. The minimizer of this search is the so-called Hartree-Fock state:

$$|\Phi^{\mathrm{HF}}\rangle = \arg\min_{\Phi} \langle\Phi|\hat{H}|\Phi\rangle. \tag{2}$$

Consider now the following λ-dependent Hamiltonian

$$\hat{H}_\lambda^{\mathrm{HF}} = \hat{T} + \hat{V}_{\mathrm{HF}} + \hat{V} + \lambda\left(\hat{V}_{ee} - \hat{V}_{\mathrm{HF}}\right) \tag{3}$$

where $\hat{V}_{\mathrm{HF}} = \sum_{i,j}^N \left(\hat{J}_j^{\mathrm{HF}}(\mathbf{x}_i) - \hat{K}_j^{\mathrm{HF}}(\mathbf{x}_i)\right)$,

$$\hat{J}_i^{\mathrm{HF}}(\mathbf{x}) = \int \frac{|\psi_i^{\mathrm{HF}}(\mathbf{x}')|^2}{|\mathbf{r}-\mathbf{r}'|}\,\mathrm{d}\mathbf{x}' \tag{4}$$

and $\hat{K}_i^{\mathrm{HF}}$, which can be defined via its action on a test function $\phi(\mathbf{x})$, reads

$$\hat{K}_i^{\mathrm{HF}}(\mathbf{x})\phi(\mathbf{x}) = \psi_i^{\mathrm{HF}}(\mathbf{x}) \int \frac{\psi_i^{\mathrm{HF}*}(\mathbf{x}')\,\phi(\mathbf{x}')}{|\mathbf{r}-\mathbf{r}'|}\,\mathrm{d}\mathbf{x}'. \tag{5}$$

The λ-dependent Hamiltonian in eq (3) is such that when $\lambda = 1$, we recover the interacting Hamiltonian [Eq.(1)], while when $\lambda = 0$, we recover the HF Hamiltonian, $\hat{H}^{\mathrm{HF}}$. $\hat{H}^{\mathrm{HF}}$ is the Hamiltonian that has the HF wave function, Φ^{HF}, as its ground state. For general λ, the ground-state (GS) wavefunction of eq (3) is denoted $\Psi_\lambda^{\mathrm{HF}}$ and the GS energy E_λ^{HF}.

Defining the correlation energy for the HF reference as

$$E_c^{\mathrm{HF}} = \langle\Psi|\hat{\mathcal{H}}|\Psi\rangle - \langle\Phi^{\mathrm{HF}}|\hat{\mathcal{H}}|\Phi^{\mathrm{HF}}\rangle, \tag{6}$$

the Hellmann-Feynman theorem on eq (3) yields

$$E_c^{\mathrm{HF}} = \int_0^1 W_\lambda^{\mathrm{HF}}\mathrm{d}\lambda \tag{7}$$

with

$$W_\lambda^{\mathrm{HF}} := \langle\Psi_\lambda^{\mathrm{HF}}|\hat{V}_{ee} - \hat{V}_{\mathrm{HF}}|\Psi_\lambda^{\mathrm{HF}}\rangle + c_0^{\mathrm{HF}}[n^{\mathrm{HF}}]. \tag{8}$$

The constant shift c_0^{HF} is equal to $U_{\mathrm{H}}[n^{\mathrm{HF}}] + E_x[\{\psi_i^{\mathrm{HF}}\}]$, where $U_{\mathrm{H}}[n] = \frac{1}{2}\int\int \frac{n(\mathbf{r})n(\mathbf{r}')}{|\mathbf{r}-\mathbf{r}'|}\mathrm{d}\mathbf{r}\mathrm{d}\mathbf{r}'$ is the mean field repulsion energy, and $E_x[\{\psi_i\}] = -\frac{1}{2}\sum_{i,j}^N \int\int \frac{\psi_i^*(\mathbf{x})\psi_j^*(\mathbf{x})\psi_i(\mathbf{x}')\psi_j(\mathbf{x}')}{|\mathbf{r}-\mathbf{r}'|}\mathrm{d}\mathbf{x}\mathrm{d}\mathbf{x}'$ is the exchange energy, which comes from evaluating the interaction operator on a Slater determinant and subtracting the mean field term.

The notation W_λ^{HF} has been adopted[31] for the adiabatic connection integrand including an additional $E_x[\{\psi_i^{\mathrm{HF}}\}]$, which is however a λ-independent quantity. The only difference between the two definitions is that when $\lambda = 0$, W_λ^{HF} of eq (8) (which is elsewhere referred to as "$W_{\lambda,c}^{\mathrm{HF}}$") is gauged to go to zero rather than to $E_x[\{\psi_i^{\mathrm{HF}}\}]$.

The small-λ expansion of $W_\lambda^{\rm HF}$ recovers the renowned Møller-Plesset series, i.e.

$$W_{\lambda\to 0}^{\rm HF} = \sum_{\rm n=2}^{\infty} {\rm n}\, E_c^{\rm MPn} \lambda^{\rm n-1}. \tag{9}$$

As for its expansion around the opposite limit, in this work, we shall only be concerned with the leading-order term, $W_\infty^{\rm HF}$,

$$W_{\lambda\to\infty}^{\rm HF} = W_\infty^{\rm HF} + o(\lambda^0), \tag{10}$$

whose explicit expression reads

$$W_\infty^{\rm HF} = E_{el}[n^{\rm HF}] + E_x[\{\psi_i^{\rm HF}\}], \tag{11}$$

with

$$E_{\rm el}[n] \equiv \min_{\{\mathbf{r}_1 \dots \mathbf{r}_N\}} \left\{ \sum_{i,j>i}^{N} \frac{1}{|\mathbf{r}_i - \mathbf{r}_j|} - \sum_{i=1}^{N} v_{\rm H}(\mathbf{r}_i;[n]) + U_{\rm H}[n] \right\}, \tag{12}$$

the minimum total electrostatic energy of N equal classical point charges $(-e)$ in a positive background with continuous charge density $(+e)n(\mathbf{r})$.

We also recall that

$$\lim_{\lambda\to\infty} \Psi_\lambda^{\rm HF} = \operatorname*{argmin}_{\Psi} \langle \Psi | \hat{H}_\infty^{\rm HF} | \Psi \rangle, \tag{13}$$

with $\hat{H}_\infty^{\rm HF} := \hat{V}_{ee} - \sum_{i,j}^{N} \sum_{\sigma_i} \hat{J}_j^{\rm HF}(\mathbf{x}_i)$[31]. Since $\hat{H}_\infty^{\rm HF}$ is a purely multiplicative operator, the square modulus of its minimizing wave function, $|\Psi_\infty^{\rm HF}|^2$, is a classical distribution in $\mathbb{R}^{3N}$ localised where $\hat{H}_\infty^{\rm HF}$ as a function of $\mathbf{r}_1, ..., \mathbf{r}_N$ attains its global minimum, i.e.,

$$|\Psi_\infty^{\rm HF}|^2 = \frac{1}{N!} \sum_{\wp=1}^{N!} \prod_{i=1}^{N} \delta(\mathbf{r}_i - \mathbf{r}_{\wp(i)}^{\rm min}). \tag{14}$$

Equation (14) essentially tells us that the particles sit at fixed positions with respect to one another, forming a perfect crystal (with translational and rotational freedom), while the permutations $\wp(i)$ account for the indistinguishability of the particles. As mentioned in the Introduction, beside the interest that the $\lambda \to \infty$ limit might raise *per se*, $W_\infty^{\rm HF}$ is used in interpolation formulas that have proven worthwhile for the determination of properties of systems at their physical ($\lambda = 1$) interaction strength (such as for the determination of interaction energies of non-covalent complexes[25]).

Let us now review the theory of the adiabatic connection typically considered in DFT: the density-fixed adiabatic connection.[11–13,35]

Consider the Levy-Lieb λ-dependent functional[36]

$$F_\lambda[n] := \min_{\Psi\to n} \langle \Psi | \hat{T} + \lambda \hat{V}_{ee} | \Psi \rangle, \tag{15}$$

with $\Psi_\lambda^{\rm KS}[n]$ the minimizer of the above search. Assuming that n is v-representable for all λ, one can write the following λ-dependent Hamiltonian:

$$\hat{H}_\lambda^{\rm KS} = \hat{T} + \lambda \hat{V}_{ee} + \hat{V}^\lambda, \tag{16}$$

where $\hat{V}^\lambda = \sum_i^N v^\lambda(\mathbf{r}_i)$, and

$$v^\lambda[n_0](\mathbf{r}) = -\frac{\delta F_\lambda[n]}{\delta n}\Big|_{n=n_0}(\mathbf{r}) \tag{17}$$

is the local external potential that enforces the prescribed density n at each λ. Defining the XC energy of KS-DFT as

$$E_{xc}^{\rm KS}[n] = F_1[n] - F_0[n] - U_{\rm H}[n], \tag{18}$$

the Hellmann-Feynman theorem on eq (15) yields

$$E_{xc}^{\rm KS}[n] = \int_0^1 W_\lambda^{\rm KS}[n] {\rm d}\lambda \tag{19}$$

with

$$W_\lambda^{\rm KS}[n] := \langle \Psi_\lambda^{\rm KS}[n] | \hat{V}_{ee} | \Psi_\lambda^{\rm KS}[n] \rangle - U_{\rm H}[n]. \tag{20}$$

A small note is that, in some sense, in DFT it is more natural to define the XC energy rather than only the correlation part. However, the exchange energy of DFT is formally analogous to that of HF, in the cases in which the KS state $\Psi_0^{\rm KS}$ is a Slater determinant, $\Phi^{\rm KS}$, something which is usually assumed. Then the correlation energy in DFT can be defined as

$$E_c^{\rm KS}[n] = E_{xc}^{\rm KS}[n] - E_x[\{\psi_i^{\rm KS}\}[n]], \tag{21}$$

where the $\psi_i^{\rm KS}$ are the orbitals that form the KS determinant.

The most conspicuous difference between the adiabatic connection formalism introduced in eq (3) and the DFT adiabatic connection is that, in this latter, the density is kept fixed along λ. In other words, there is a subtle dependence on λ sneaking in via the $\hat{V}^\lambda$ operator. As a consequence, while the MP AC integrand corresponds to the derivative of the λ-dependent energy (minus a shift), i.e.,

$$W_\lambda^{\rm HF}[n^{\rm HF}] = \frac{\rm d}{{\rm d}\lambda} E_\lambda^{\rm HF}[n^{\rm HF}] + c_0^{\rm HF}[n^{\rm HF}], \tag{22}$$

$W_\lambda^{\rm KS}$ is rather the derivative of F_λ (minus a shift):

$$W_\lambda^{\rm KS}[n] = \frac{\rm d}{{\rm d}\lambda} F_\lambda[n] + c_0^{\rm KS}, \tag{23}$$

with $c_0^{\rm KS} = -U_{\rm H}[n]$. In turn, F_λ is also equal to $E_\lambda^{\rm KS}[n] - V_\lambda[n]$, with $E_\lambda^{\rm KS}$ the GS energy of Hamiltonian (16) and $V_\lambda[n] := \langle \Psi_\lambda^{\rm KS}[n] | \hat{V}^\lambda | \Psi_\lambda^{\rm KS}[n] \rangle$. By reshuffling eq (16), one realizes that the fluctuation potential – that is, the operator which is turned on by λ – has the form $\left(\hat{V}_{ee} + \frac{\hat{V}^\lambda - \hat{V}^{\lambda=0}}{\lambda}\right)$. Then, the small-$\lambda$ expansion of $W_\lambda^{\rm KS}$,[37,38]

$$W_{\lambda\to 0}^{\rm KS}[n] = E_x[\{\psi_i^{\rm KS}[n]\}] + \sum_{\rm n=2}^{\infty} {\rm n}\, E_c^{\rm GLn} \lambda^{\rm n-1}, \tag{24}$$

contains also the order-by-order expansion of the fluctuation potential inside the perturbation series coefficients E_c^{GLn}, adding a layer of complexity to the usual MP expressions. The n = 2 term reads

$$E_c^{\mathrm{GL2}}[n] = \sum_{i=1}^{\infty} \frac{|\langle \Phi^{\mathrm{KS}}|\hat{V}_{ee} - \sum_{j=1}^{N} v_{\mathrm{H}x}(\mathbf{r}_j)|\Phi_i^{\mathrm{KS}}\rangle|^2}{E_0^{\mathrm{KS}} - E_{0,i}^{\mathrm{KS}}}, \quad (25)$$

where $v_{\mathrm{H}x} = v_{\mathrm{H}} + v_x$ with $v_x = \frac{\delta E_x[\{\psi_i^{\mathrm{KS}}[n]\}]}{\delta n}\Big|_{n=n_0}$ and Φ_i^{KS} and $E_{0,i}^{\mathrm{KS}}$ are the excited KS states and energies. The explicit computation of any subsequent term seems absent from the literature.

The leading order of the large-λ expansion of W_λ^{KS} is also a constant,[23] analogously to eq (10):

$$W_{\lambda\to\infty}^{\mathrm{KS}}[n] = W_\infty^{\mathrm{KS}}[n] + o\left(\lambda^{-\frac{1}{2}}\right). \quad (26)$$

The asymptotic wavefunction in the DFT adiabatic connection is defined as

$$\Psi_\infty^{\mathrm{KS}} = \mathrm{argmin}_{\Psi\to n}\langle\Psi|\hat{H}_\infty^{\mathrm{KS}}|\Psi\rangle, \quad (27)$$

with $\hat{H}_\infty^{\mathrm{KS}} = \hat{V}_{ee} + \hat{V}^\infty$ and where $\hat{V}^\infty$ is the N-electron sum of the one-body operator,

$$v^\infty[n_0](\mathbf{r}) = -\frac{\delta F_\infty[n]}{\delta n}\Big|_{n=n_0}, \quad (28)$$

with $F_\infty[n] := \lim_{\lambda\to\infty}\frac{F_\lambda[n]}{\lambda}$. In a way reminiscent of eq (14) but heavily complicated by the density constraint, $\left|\Psi_\infty^{\mathrm{KS}}\right|^2$ is a semi-classical distribution

$$\left|\Psi_\infty^{\mathrm{KS}}\right|^2 = \frac{1}{N!}\sum_{\wp=1}^{N!}\int d\mathbf{s}\frac{n(\mathbf{s})}{N}\prod_{i=1}^{N}\delta\left(\mathbf{r}_i - \mathbf{f}_{\wp(i)}(\mathbf{s})\right), \quad (29)$$

where the co-motion functions $\mathbf{f}_i$ are mathematical objects which parameterize the set of all configurations where $\hat{H}_\infty^{\mathrm{KS}}$ is minimum. There are $N-1$ non-trivial co-motion functions which provide the position of $N-1$ particles, given the position of a reference one.

Note the difference between Eqs. (14) and (29) : whereas $\left|\Psi_\infty^{\mathrm{HF}}\right|^2$ is a perfect crystal with well defined positions, $\left|\Psi_\infty^{\mathrm{KS}}\right|^2$ is rather a superposition of infinitely many cristals, since the $N-1$ particle positions depend parametrically on the position of a single one which varies freely (for a more focused description of the strong-interaction limit of DFT, the interested reader is referred to references 23, 39–42).

Finally, we recall that, using the Legendre transform formulation of Lieb,[43] it has been shown[31] that, for a given density,

$$W_\infty^{\mathrm{HF}}[n] \le W_\infty^{\mathrm{KS}}[n]. \quad (30)$$

Throughout this work, we will use the superscript "SD" to indicate both the KS and the HF versions of a given quantity. For example, with E_c^{SD}, we mean E_c^{HF} and/or E_c^{KS}.

B. The Hubbard Dimer

The Hubbard model is often used to test new methods and concepts in chemistry and physics because its Hamiltonian is extremely simple compared to physical systems (atoms and molecules), while still incorporating many of the correlation effects in such systems. Its two-site version, considered in this work, reads:

$$\hat{\mathcal{H}} = \hat{\mathcal{T}} + \hat{\mathcal{U}} + \hat{\mathcal{V}} \quad (31)$$

where

$$\hat{\mathcal{T}} = -t\sum_\sigma\left(\hat{a}_{0\sigma}^\dagger\hat{a}_{1\sigma} + \hat{a}_{1\sigma}^\dagger\hat{a}_{0\sigma}\right) \quad (32)$$

$$\hat{\mathcal{U}} = U\sum_{i=0,1}\hat{n}_{i\uparrow}\hat{n}_{i\downarrow} \quad (33)$$

$$\hat{\mathcal{V}} = \sum_{i=0,1} v_i\hat{n}_i, \quad (34)$$

$\hat{a}^\dagger$, $\hat{a}$ are the usual creation and annihilation operators, $\sigma = \uparrow,\downarrow$ labels the spin of the particles, $i = 0, 1$ labels the two sites, and $\hat{n}_{i\sigma} = \hat{a}_{i\sigma}^\dagger\hat{a}_{i\sigma}$ and $\hat{n}_i = \hat{n}_{i\sigma} + \hat{n}_{i\bar{\sigma}}$ (with $\bar{\sigma}$ being the spin opposite to σ) are the occupation operators. The reduced variables $u = \frac{U}{2t}$ and $\delta v = \frac{\Delta v}{2t}$, with $\Delta v = v_1 - v_0$, fully determine the eigenstates of the Hamiltonian (31). Given this, the hopping parameter t is set to 1/2 throughout the paper and the gauge, i.e. $c = v_0 + v_1$, to zero, as is customary.[44] Furthermore, we consider the dimer at "half-filling," which means that the sum of the expectation value of the occupation operators on each site is set to two (i.e., $n_0 + n_1 = 2$) and restrict ourselves to singlet states ($S_z = 0$). The site occupation difference Δn corresponds to the electron probability density in the model and is defined as the expectation value of the difference between the site-occupation operators, $\Delta n = \langle\Psi|\hat{n}_1 - \hat{n}_0|\Psi\rangle$. The three-dimensional Hilbert space is represented in the basis $|0\uparrow 0\downarrow\rangle, |1\uparrow 1\downarrow\rangle$, and $\frac{1}{\sqrt{2}}(|0\uparrow 1\downarrow\rangle - |0\downarrow 1\uparrow\rangle)$. Note that all energy terms are symmetric with respect to the change in sign of Δv, while the sign of the site-occupation difference is opposite to that of the external potential difference. We call $\epsilon(U, \Delta v)$ the ground-state energy associated with Hamiltonian (31).

The restricted Hartree-Fock Hamiltonian for this model can be written as:[45]

$$\hat{\mathcal{H}}^{\mathrm{RHF}} = \hat{\mathcal{T}} + \hat{\tilde{\mathcal{V}}}, \quad (35)$$

with $\hat{\tilde{\mathcal{V}}} = \sum_{i=0,1}\tilde{v}_i\hat{n}_i$ and $\tilde{v}_i = v_i + U\frac{n_i^{\mathrm{HF}}}{2}$. The symbol n_i^{HF} indicates the HF site occupation on each site (as converged to its stationary point), and $U\frac{n_i^{\mathrm{HF}}}{2}$ is the site mean field potential. Note that, because $n_0^{\mathrm{HF}} + n_1^{\mathrm{HF}} = 2$, setting $v_0 + v_1 = 0$ in eq (31) forces the sum of $\tilde{v}_i$ to give $\tilde{v}_0 + \tilde{v}_1 = U$.

II. MP AND DFT ADIABATIC CONNECTIONS FOR THE HUBBARD DIMER

Using Eqs. (31) and (35), the Møller-Plesset adiabatic connection [eq (3)] for the Hubbard dimer reads

$$\begin{aligned}\hat{H}_\lambda^{\mathrm{HF}} &= \hat{\mathcal{T}} + \sum_i \tilde{v}_i \hat{n}_i + \lambda U \sum_i \left(\hat{n}_{i\uparrow}\hat{n}_{i\downarrow} - \frac{n_i^{\mathrm{HF}}}{2}\hat{n}_i \right) \\ &= \hat{\mathcal{T}} + \lambda U \sum_i \hat{n}_{i\uparrow}\hat{n}_{i\downarrow} + \sum_i v_i^{\lambda,\mathrm{HF}} \hat{n}_i, \end{aligned} \tag{36}$$

where in the second line we have introduced the λ-dependent external potential, $v_i^{\lambda,\mathrm{HF}}$, defined as

$$v_i^{\lambda,\mathrm{HF}} := \tilde{v}_i - \lambda U \frac{n_i^{\mathrm{HF}}}{2}, \tag{37}$$

and where the gauge – defined as $c^{\lambda,\mathrm{HF}} = v_0^{\lambda,\mathrm{HF}} + v_1^{\lambda,\mathrm{HF}}$ – depends linearly on λ:

$$c^{\lambda,\mathrm{HF}} = U(1-\lambda). \tag{38}$$

The associated λ-dependent ground state, $\Psi_\lambda^{\mathrm{HF}}$, can be calculated explicitly for any pair of interaction parameter and external potential, $\{U, \Delta v\}$. Consequently, it is also possible to study the λ-dependent behaviour of relevant quantities such as the adiabatic connection integrand, W_λ^{HF} (section III A), and the site occupation difference, $\Delta n_\lambda^{\mathrm{HF}}$ (section III C), analytically as functions of the variables $\{U, \Delta v\}$. They can also be expressed analytically as functions of Δn^{HF}, the HF site occupation difference, in place of Δv, as the function $f : \Delta v \to \Delta n^{\mathrm{HF}}$ is analytically invertible.[45]

The MP adiabatic connection integrand for our model system reads

$$W_\lambda^{\mathrm{HF}} = \langle \Psi_\lambda^{\mathrm{HF}} | \hat{\mathcal{U}} - U \sum_i \frac{n_i^{\mathrm{HF}}}{2} \hat{n}_i | \Psi_\lambda^{\mathrm{HF}} \rangle + \frac{U}{2} \left(1 + \left(\frac{\Delta n^{\mathrm{HF}}}{2} \right)^2 \right), \tag{39}$$

where the term in the Dirac brakets is simply $\frac{\mathrm{d}\, E_\lambda^{\mathrm{HF}}}{\mathrm{d}\lambda}$ and the remainder is c_0^{HF} for the Hubbard dimer, i.e. the shift which makes $W_0^{\mathrm{HF}} = 0$.

As for the density-fixed adiabatic connection, even in the simple setting of the asymmetric Hubbard dimer, the λ-dependent potential that keeps the density fixed cannot be determined in closed form. However, it can be computed quite efficiently by using Lieb's formulation,[43]

$$\Delta v^{\lambda,\mathrm{KS}}(U, \Delta n) = \arg\max_{\Delta v} \left(\epsilon(\lambda U, \Delta v) - \frac{\Delta v}{2} \Delta n \right), \tag{40}$$

with $\Delta v^{\lambda,\mathrm{KS}} = v_1^{\lambda,\mathrm{KS}} - v_0^{\lambda,\mathrm{KS}}$ and the usual gauge $v_1^{\lambda,\mathrm{KS}} + v_0^{\lambda,\mathrm{KS}} = 0$. With $\Delta v^{\lambda,\mathrm{KS}}$, we construct the λ-dependent Hamiltonian of the density-fixed adiabatic connection [eq (16)] for the Hubbard dimer,

$$H_\lambda^{\mathrm{KS}} = \hat{\mathcal{T}} + \lambda U \sum_i \hat{n}_{i\uparrow}\hat{n}_{i\downarrow} + \frac{\Delta v^{\lambda,\mathrm{KS}}(U, \Delta n)}{2} (\hat{n}_1 - \hat{n}_0), \tag{41}$$

and the corresponding AC integrand [eq (20)],

$$W_\lambda^{\mathrm{KS}} = \langle \Psi_\lambda^{\mathrm{KS}} | \hat{\mathcal{U}} | \Psi_\lambda^{\mathrm{KS}} \rangle + \frac{U}{2} \left(1 + \left(\frac{\Delta n}{2} \right)^2 \right), \tag{42}$$

where $\Psi_\lambda^{\mathrm{KS}}$ is the λ-dependent ground state associated with the Hamiltonian given in eq (41). Differently than for eq (39), the term in Dirac brackets in (42) is not the derivative of the total energy with respect to λ, but rather the derivative of F^λ [eq (15)], which in this setting reads

$$F^\lambda(U, \Delta n) = \langle \Psi_\lambda^{\mathrm{KS}} | \hat{\mathcal{T}} + \lambda U \sum_i \hat{n}_{i\uparrow}\hat{n}_{i\downarrow} | \Psi_\lambda^{\mathrm{KS}} \rangle. \tag{43}$$

Equation (17) then translates into

$$\frac{\Delta v^{\lambda,\mathrm{KS}}(U, \Delta n)}{2} = -\frac{\partial F^\lambda(U, \Delta n)}{\partial \Delta n}. \tag{44}$$

Both AC integrands are defined in such a way that

$$E_c^{\mathrm{SD}} = \int_0^1 W_\lambda^{\mathrm{SD}} \mathrm{d}\lambda \tag{45}$$

with SD=HF, KS and $E_c^{\mathrm{SD}} = \langle \Psi | \hat{\mathcal{H}} | \Psi \rangle - \langle \Psi_0^{\mathrm{SD}} | \hat{\mathcal{H}} | \Psi_0^{\mathrm{SD}} \rangle$ (compare Eqs.(6) and (19), (21)).

Introducing a generalized λ-dependent correlation energy (not unusual in DFT[37,46]) as

$$E_{c,\lambda}^{\mathrm{SD}} = \int_0^\lambda W_{\lambda'}^{\mathrm{SD}} \mathrm{d}\lambda', \tag{46}$$

where $E_{c,1}^{\mathrm{SD}} = E_c^{\mathrm{SD}}$, in the Hubbard dimer setting, one finds

$$E_{c,\lambda}^{\mathrm{SD}}(U, \Delta n) = E_c^{\mathrm{SD}}(\lambda U, \Delta n) \tag{47}$$

for both types of correlation energies.

III. RESULTS

In this section, we present the analytical and numerical results obtained for the MP and DFT adiabatic connections, respectively.

A. Shapes of the two adiabatic connection integrands

In Figure 1, we report the two AC integrands, Eqs. (39) and (42), in the $0 < \lambda < 1$ range (first column) and for λ large enough for both AC integrands to converge to their asymptotic values (second column), for selected values of U and $|\Delta v|$ parameters. For $U = 1$, we take $|\Delta v| = 10, 1, 0.1$, while for $U = 0.1$ and $U = 10$ we consider only $|\Delta v| = U$.

The ratio between U and $|\Delta v|$ is an important factor in determining the amount and the type of correlation present in a given calculation. A dominant U will favor

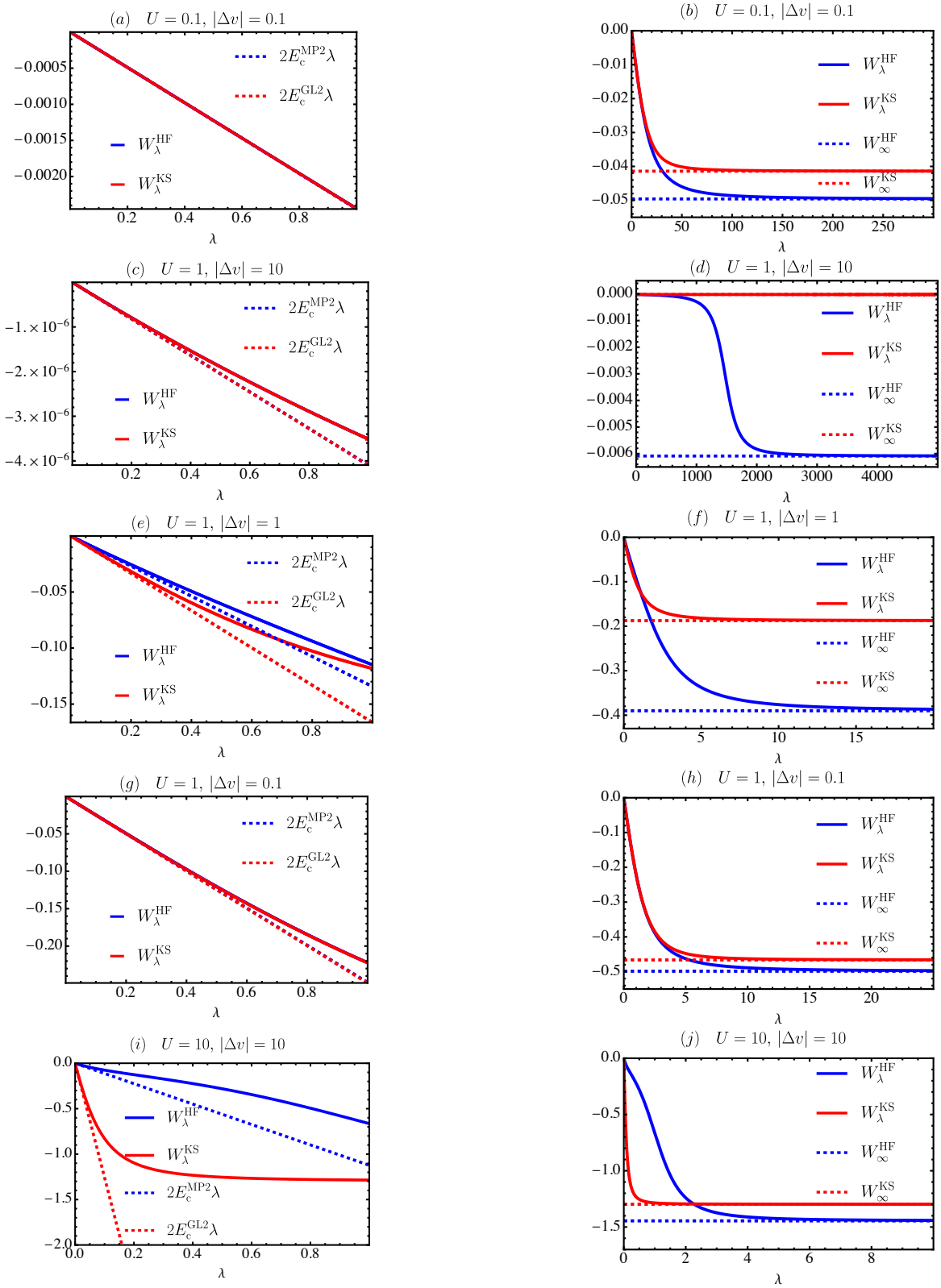

FIG. 1: Shapes of the two AC integrands, $W_\lambda^{\rm KS}$ (solid red) and $W_\lambda^{\rm HF}$ (solid blue), at different correlation regimes. In the left column, λ ranges between 0 and 1 and $2\,E_{\rm c}^{\rm GL2}\,\lambda$ (dashed red) and $2\,E_{\rm c}^{\rm MP2}\,\lambda$ (dashed blue) are plotted for comparison. In the right column, the range extends to λ large enough for both AC integrands to converge to their asymptotic values, $W_\infty^{\rm KS}$ (dashed red) and $W_\infty^{\rm HF}$ (dashed blue). For illustrative purposes, the values of $U/|\Delta v|$ selected are 0.1, 1, and 10 (as per the plots' labels). For $U = 0.1$ and $|\Delta v| = 0.1$ both AC integrands show an almost perfectly linear behaviour within the relevant λ range from 0 to 1 and are barely distinguishable from one another [panel (a)]. At large λ, their behaviour does not differ very much quantitatively and looks very similar qualitatively [(b)]. In the other panels with $U/|\Delta v| = 1$ [(e) and (i)] $W_\lambda^{\rm KS}$ and $W_\lambda^{\rm HF}$ differ visibly in the range $0 \leq \lambda \leq 1$. Moreover, in (i) there is a striking *qualitative* difference: the MP adiabatic connection integrand changes curvature twice. Though not clearly visible from the plot, $W_\lambda^{\rm HF}$ starts convex, turning concave around $\lambda \approx 0.22$ and turning convex again around $\lambda \approx 0.99$. The change from concave to convex of $W_\lambda^{\rm HF}$ is clearly visible in panel (d), where the ratio $U/|\Delta v| = 0.1$ and the system is "weakly interacting". Finally, note that $W_\lambda^{\rm HF}$ starts always above $W_\lambda^{\rm KS}$ and, in the cases plotted, ends below $W_\lambda^{\rm KS}$, but the two curves cross beyond $\lambda = 1$. See main text for more discussion.

localization of each "particle" on a single site (strong interaction or small $|\Delta n|$), whereas a dominant $|\Delta v|$ will favor both particles on one site (weak interaction or large $|\Delta n|$). Nevertheless, the absolute magnitude of U is also important. For example, in the first panel where $U/|\Delta v| = 1$ and $U = 0.1$, both AC curves show an almost perfect linear behavior in the relevant range between 0 and 1. However, for the same ratio and $U = 1$ and 10 [panels (e) and (i)], the AC integrands deviate significantly from linearity (increasingly for larger U). An "almost linear" AC integrand is considered as an example of *dynamical* correlation whereas a markedly non-linear one as *static* correlation (see e.g. Refs. 27 and 47). This difference is often assessed globally by looking at the expansion of the correlation energy at small λ,

$$\lim_{\lambda\to 0} E^{\mathrm{SD}}_{c,\lambda} = \lambda^2 E^{\mathrm{SD}}_{c,(2)} + o(\lambda^2). \tag{48}$$

In particular, using only the leading order coefficient, $E^{\mathrm{SD}}_{c,(2)}$, to approximate the correlation energy corresponds to approximating the integrand W^{SD}_λ as a linear function with slope $2 * E^{\mathrm{SD}}_{c,(2)}$. This coefficient is typically referred to as MP2 and GL2 correlation energies, for the MP and the DFT adiabatic connection, respectively (see Eqs. (9) and (24)). MP2 and GL2 correlation energies can be used as approximations of the total correlation energy and their performance can be measured through their relative error:

$$\text{rel. err. SD} = \left|\frac{E^{\mathrm{SD}}_{c,(2)} - E^{\mathrm{SD}}_{\mathrm{c}}}{E^{\mathrm{SD}}_{\mathrm{c}}}\right| \times 100. \tag{49}$$

From Figure 1, panel (g), we see that a dominant U does not imply that the AC integrand curve is far from linear or that the relative error is big. In this case, one may talk about "strong dynamical correlation." Indeed the relative error for $U = 1$ and $|\Delta v| = 0.1$ is 6.0% and 6.1% for the MP and the DFT adiabatic connection, respectively. More quantitative data can be found in Table I, which reports the values of interacting and HF site-occupation difference, correlation energy, $E^{\mathrm{SD}}_{c,(2)}/E^{\mathrm{SD}}_c$ ratio, and relative error, for $U/|\Delta v| = 0.1$, 1, 10 and $U = 0.1$, 1, 10. The quantity $(1 - \lambda^{\mathrm{SD}}_{\mathrm{ext}})$, which will be the focus of section III B, is also reported.

Qualitatively, we observe a convex DFT adiabatic connection integrand across the full parameter space of the Hubbard dimer. This result adds to the long list of highly accurate numerical evidence of the (piecewise) convexity of this curve,[27,47–55] something which has yet to be proven. On the contrary, for the MP adiabatic connection, cases have been reported where the integrand is rather concave at small λ.[4,27,34] However, in the Hubbard dimer setting, we find that the MP adiabatic connection integrand may change curvature twice. In particular, for any $U > 0$, we observe a double change of curvature (DCOC) for a continuous range of Δv beyond a certain value that depends on U.

For example, in panel (i), W^{HF}_λ (blue solid curve) starts convex, turning concave around $\lambda \approx 0.22$ and turning convex again around $\lambda \approx 0.99$. The change in curvature from concave to convex of W^{HF}_λ is extremely visible in panel (d), where Δv is dominating and the system is in the weak-interaction regime. Note that the integrand of eq (39) is convex (i.e. lying *above* its tangent) around $\lambda \to 0$ for any pair of $\{U, \Delta v\}$. In fact, in the cases in which W^{HF}_λ is concave in some region [e.g., for the cases plotted in panels (d) and (i-j)], the MP adiabatic connection integrand still starts convex, having to change curvature an even number of times to reach a bound asymptotic value. This is at variance with the mentioned cases where a change of curvature had been previously observed, for which the adiabatic connection integrand is concave (i.e. lying *below* its tangent) around zero (the He atom is one such example).

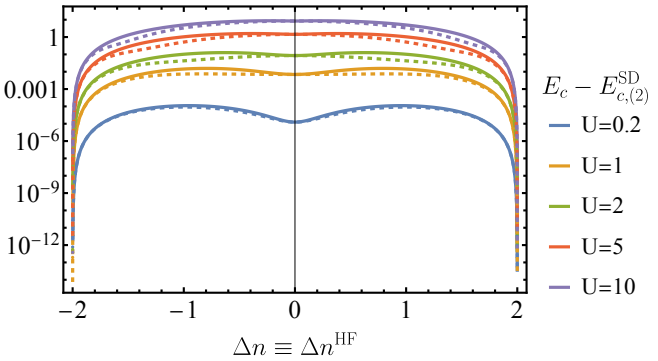

FIG. 2: Difference between total correlation energy and its second-order expansion, $E_c - E^{\mathrm{SD}}_{c,(2)}$, with SD = HF (dashed) and KS (solid) for $U = 0.2, 1, 2, 5, 10$ as functions of the HF and interacting site-occupation difference, respectively. The difference is always positive across all the site-occupation domain, meaning that the second-order expansion always overshoots the correlation energy (the scale is logarithmic to help readability).

Oftentimes, whether E^{MP2}_c overestimates or underestimates the exact correlation energy E^{HF}_c has been considered[27,31,34] as an indicator for the convex or concave nature of the curve at the origin; however, this reasoning only holds if the curvature changes at most once in the range $0 \le \lambda \le 1$, something which our findings show to not always hold true. Nonetheless, in the Hubbard dimer setting, we find that E^{MP2}_c always overestimates in magnitude the correlation energy, in line with the naive expectation that an AC integrand that is convex at small λ indicates an E^{MP2}_c that overshoots the correlation energy (see Figure 2).

In conclusion, in the Hubbard dimer model at any correlation regime we have

$$|E^{\mathrm{SD}}_{c,(2)}| \ge |E^{\mathrm{SD}}_{\mathrm{c}}| \tag{50}$$

for "SD" either KS (AC integrand convex everywhere) or HF (AC integrand convex for $\lambda = 0$).

Moreover, as noted in Ref. 45, $E^{\mathrm{SD}}_{c,(2)}$ has formally the

same expression in the two adiabatic connections, namely

$$E_{c,(2)}^{\mathrm{SD}} = -\frac{1}{256}U^2\left(4-x^2\right)^{5/2} \tag{51}$$

with $x = \Delta n^{\mathrm{SD}}$. In turn, $|\Delta n^{\mathrm{HF}}| \geq |\Delta n^{\mathrm{KS}}|$ and $0 \leq |\Delta n^{\mathrm{SD}}| < 2$. Then, for a given $\{U, \Delta v\}$ pair,

$$|E_{\mathrm{c}}^{\mathrm{GL2}}| \geq |E_{\mathrm{c}}^{\mathrm{MP2}}|. \tag{52}$$

The thorny question that remains is what causes the observed double change of curvature in W_λ^{HF} (and whether it can be expected in Coulomb systems). As seen, the DCOC in the Hubbard dimer setting occurs in a continuous range of $|\Delta v|$, starting from $|\Delta v|$ around U to $|\Delta v| \to \infty$, i.e., starting around the switch between strong- and weak-interaction regime and persisting in the weak-interaction regime. Although we have not found a simple explanation for the DCOC, we highlight in the following some aspects of the MP adiabatic connection that might endow it with such "extra flexibility" compared to the DFT one.

Let us start by analyzing the leading coefficient in the weak-interaction expansion of the correlation energy.

Despite the formal equivalence of $E_{c,(2)}^{\mathrm{SD}}$in the two adiabatic connections [eq (51)], how this energy term is parsed into the individual components is quite different between the DFT and the MP case. To see this, let us introduce the definition of the individual components of the total correlation energy as

$$U_{c,\lambda}^{\mathrm{SD}} = \langle\Psi_\lambda^{\mathrm{SD}}|\lambda\hat{\mathcal{U}}|\Psi_\lambda^{\mathrm{SD}}\rangle - \langle\Psi_0^{\mathrm{SD}}|\lambda\hat{\mathcal{U}}|\Psi_0^{\mathrm{SD}}\rangle \tag{53a}$$

$$T_{c,\lambda}^{\mathrm{SD}} = \langle\Psi_\lambda^{\mathrm{SD}}|\hat{\mathcal{T}}|\Psi_\lambda^{\mathrm{SD}}\rangle - \langle\Psi_0^{\mathrm{SD}}|\hat{\mathcal{T}}|\Psi_0^{\mathrm{SD}}\rangle \tag{53b}$$

$$\begin{aligned} V_{c,\lambda}^{\mathrm{SD}} &= \langle\Psi_\lambda^{\mathrm{SD}}|\hat{\mathcal{V}^{\lambda,\mathrm{SD}}}|\Psi_\lambda^{\mathrm{SD}}\rangle - \langle\Psi_0^{\mathrm{SD}}|\hat{\mathcal{V}}|\Psi_0^{\mathrm{SD}}\rangle \\ &= \frac{\Delta v^{\lambda,\mathrm{SD}}}{2}\left(\Delta n^{\lambda,\mathrm{SD}} - \Delta n^{\mathrm{SD}}\right) \end{aligned} \tag{53c}$$

With $\hat{\mathcal{V}^{\lambda,\mathrm{SD}}} = \sum_i v_i^{\lambda,SD}\hat{n}_i$. (Note that, for each individual contribution to correlation, the analogue of eq (47) holds true.) The $\lambda \to 0$ expansion of these terms looks formally identical to eq (48) and in both HF and KS references, we have

$$E_{c,(2)}^{\mathrm{SD}} = \frac{U_{c,(2)}^{\mathrm{SD}}}{2}. \tag{54}$$

However, while in DFT

$$T_{c,(2)}^{\mathrm{KS}} = -\frac{U_{c,(2)}^{\mathrm{KS}}}{2} \tag{55}$$

and $T_{c,(2)}^{\mathrm{KS}} + U_{c,(2)}^{\mathrm{KS}} = E_{c,(2)}^{\mathrm{KS}}$, in the MP adiabatic connection, the non-zero $V_{c,\lambda}^{\mathrm{HF}}$ complicates the expression significantly. There, we have

$$T_{c,(2)}^{\mathrm{HF}} = \frac{\left(4-5x^2\right)\left(4-x^2\right)^{5/2}}{1024} \tag{56a}$$

$$V_{c,(2)}^{\mathrm{HF}} = \frac{5x^2\left(4-x^2\right)^{5/2}}{1024}, \tag{56b}$$

such that

$$T_{c,(2)}^{\mathrm{HF}} + V_{c,(2)}^{\mathrm{HF}} = -\frac{U_{c,(2)}^{\mathrm{HF}}}{2}. \tag{57}$$

The presence of $V_{c,\lambda}^{\mathrm{HF}}$ appears to be possibly "the" crucial difference between the DFT and the MP adiabatic connection.

Another way to rephrase this crucial difference is that the DFT AC integrand only contains the two-body operator, whereas the MP AC integrand also contains the one-body operator corresponding to the external potential correction [compare Eqs. (42) and (39)].

B. Analysis of correlation indicators and accuracy predictors

In this section, we calculate the correlation indicator λ_{ext},[27,55] used in the context of adiabatic connection methods, in the full parameter space of our model for both adiabatic connections. This indicator is defined as

$$\lambda_{\mathrm{ext}}^{\mathrm{SD}} := \frac{W_1^{\mathrm{SD}}}{2\,E_{c,(2)}^{\mathrm{SD}}}. \tag{58}$$

This is a dimensionless quantity that determines the λ value at which the linear curve, given by the slope of W_λ^{SD} at $\lambda = 0$, crosses the constant curve corresponding to $W_{c,1}^{\mathrm{SD}}$, where $W_{c,1}^{\mathrm{SD}} = W_1^{\mathrm{SD}} - W_0^{\mathrm{SD}}$. (However, in our model, $W_0^{\mathrm{SD}} = 0$, therefore $W_{c,1}^{\mathrm{SD}} = W_1^{\mathrm{SD}}$.)

By definition, $\lambda_{\mathrm{ext}}^{\mathrm{SD}} = 1$ means that the curve $2\,E_{c,(2)}^{\mathrm{SD}}\lambda$ crosses the constant W_1^{SD} exactly at $\lambda = 1$. In the assumption that the MP AC integrand changes curvature at most once in the relevant range of λ between zero and one, $\lambda_{\mathrm{ext}}^{\mathrm{SD}} = 1$ is indeed enough to say that the second-order energy expansion recovers all the correlation energy and that the AC integrand is linear and fully "dynamically correlated." Thus, how much $\lambda_{\mathrm{ext}}^{\mathrm{SD}}$ differs from one, i.e., the quantity $|1 - \lambda_{\mathrm{ext}}^{\mathrm{SD}}|$, has been considered as a predictor of the accuracy of the second-order perturbation estimate of the correlation energy. This can be measured using the relative error defined in eq (49). However, the possible presence of more than one change of curvature invalidates this deduction. Our results therefore raise the interesting question of whether the quantity $|1 - \lambda_{\mathrm{ext}}^{\mathrm{HF}}|$ remains a meaningful predictor of the corresponding relative error.

In addition to this possible issue arising from the double change of curvature, the correspondence between a certain non-zero value of $|1 - \lambda_{\mathrm{ext}}^{\mathrm{SD}}|$ and the relative error is not obvious. Even with the assumption that there is at most *one* change of curvature in the relevant range of λ between 0 and 1 holding (and therefore $\lambda_{\mathrm{ext}}^{\mathrm{SD}} = 1$ implies that the relative error is exactly zero), it is useful to extend our analysis to the DFT adiabatic connection as well, despite it appearing to give a convex integrand in the full parameter space of our model, to further clarify this correspondence and its applicability.

A technical aspect worth mentioning is that the accuracy predictor $|1 - \lambda_{\mathrm{ext}}|$, introduced in reference 27, has

	$U=0.1$			$U=1$			$U=10$		
$U/\lvert\Delta v\rvert$	0.1	1	10	0.1	1	10	0.1	1	10
$\lvert\Delta v\rvert$	1	0.1	0.01	10	1	0.1	100	10	1
$\Delta n^{\rm HF}$	1.363	0.181	0.018	1.988	0.938	0.100	2.000	1.686	0.182
Δn	1.3632	0.180	0.018	1.988	0.775	0.068	2.000	0.981	0.004
$\lvert E_{\rm c}^{\rm HF}\rvert$	2.5×10^{-4}	1.2×10^{-3}	1.3×10^{-3}	1.8×10^{-6}	0.060	0.117	1.9×10^{-9}	0.305	4.054
$\lvert E_{\rm c}^{\rm KS}\rvert$	2.5×10^{-4}	1.2×10^{-3}	1.3×10^{-3}	1.8×10^{-6}	0.068	0.117	1.9×10^{-9}	1.145	4.098
$E_{\rm c}^{\rm MP2}/E_{\rm c}^{\rm HF}$	1.033	1.001	1.001	1.109	1.125	1.060	1.111	1.843	3.020
$E_{\rm c}^{\rm GL2}/E_{\rm c}^{\rm KS}$	1.035	1.001	1.001	1.109	1.230	1.061	1.111	5.483	3.050
rel. err. HF	3.3%	0.1%	0.1%	10.9%	12.5%	6.0%	11.1%	84.3%	202%
rel. err. KS	3.5%	0.1%	0.1%	10.9%	23.0%	6.1%	11.1%	448.3%	205%
$1-\lambda_{\rm ext}^{\rm HF}$	0.047	0.002	0.001	0.142	0.144	0.106	0.145	0.409	0.802
$1-\lambda_{\rm ext}^{\rm KS}$	0.050	0.003	0.001	0.143	0.289	0.108	0.145	0.898	0.804

TABLE I: HF and KS site occupation differences, $\Delta n^{\rm HF}$ and Δn, correlation energies, $E_{\rm c}^{\rm HF}$ and $E_{\rm c}^{\rm KS}$, ratio between second-order and exact correlation energy, $E_{\rm c}^{\rm MP2}/E_{\rm c}^{\rm HF}$ and $E_{\rm c}^{\rm GL2}/E_{\rm c}^{\rm KS}$, relative error on correlation energy, "rel. err. SD" [eq (49)] and $(1-\lambda_{\rm ext}^{\rm SD})$ [see eq (58)], for $U=0.1$, 1, 10 and $U/|\Delta v|=0.1$, 1, 10. This choice corresponds to moving from "weak" to "strong interaction" regime for a fixed U, as can be appreciated from the decreasing values of Δn and $\Delta n^{\rm HF}$ and the increasing values of $E_{\rm c}^{\rm HF}$ and $E_{\rm c}^{\rm KS}$.

been applied in the context of the MP adiabatic connection in terms of a modified correlation indicator, $\lambda_{\rm ext}^{\rm SPL}$. "SPL" refers to the Seidl-Perdew-Levy formula,[20] which approximates the DFT AC integrand using a convex interpolant and thus serves as a means to approximate $W_{c,1}$ (which is typically unknown in its exact form). This interpolation formula has proven surprisingly useful for molecular applications when used in the framework of the MP AC.[25–28,56] In the above applications, however, the SPL interpolation formula is used as a correction not to absolute energies, but rather to energy differences, as its accuracy has been found to be poor for the former but satisfactory for the latter. Thus, also the use of the accuracy predictor, if one uses the SPL or similar formulas to approximate $W_{c,1}$, is recommended in terms of energy differences and not absolute energies. In the present work, however, $W_{c,1}$ (or W_1) can be calculated *exactly* and therefore can be used directly to construct $|1-\lambda_{\rm ext}|$ for absolute energies, in line with the original idea[55] that the relative error [eq (49)] increases as $\lambda_{\rm ext}$ deviates from one. Finally note that, by virtue of eq (50), $\lambda_{\rm ext}\leq 1$ and the modulus can be ignored in the context of this work.

In Figure 3, we plot the relative error on the y-axis and $|1-\lambda_{\rm ext}|$ on the x-axis for the same $\{U,\Delta n\}$ pair, exploring $U=0.1$, 1, 10 and the full site occupation difference range, $0\leq\Delta n\leq 2$, within the MP (left column) and the DFT (right) adiabatic connections. From the plots, we see that the relative error is not a function of the quantity $|1-\lambda_{\rm ext}|$; however, this quantity does appear to be a significant factor in determining the relative error. Moreover, although there is a somewhat commensurate behavior between the two columns, there are both quantitative and qualitative differences between the results for the MP and DFT adiabatic connections. Quantitatively, the error given by GL2 is both more sensitive to U and typically larger than the error given by MP2. The same is true if we look at $|1-\lambda_{\rm ext}^{\rm KS}|$ and $|1-\lambda_{\rm ext}^{\rm HF}|$. This trend can be more easily appreciated by looking at Table II where the mean, μ, of the distribution of the relative error as well as of the $|1-\lambda_{\rm ext}|$ for each given U over the full Δn range is calculated, together with their standard deviations, σ. In particular, we see that $\mu_{\rm rel.err.KS}>\mu_{\rm rel.err.HF}$ and $\mu_{|1-\lambda_{\rm ext}^{\rm KS}|}>\mu_{|1-\lambda_{\rm ext}^{\rm HF}|}$ in all cases, and we see that the increment of the KS quantities with U is much larger than that of the HF quantities. The qualitative differences between the two columns of Figure 3 emerge by looking at how smaller Δn values are placed with respect to the relative error for the cases where fixed $|1-\lambda_{\rm ext}|$ yields two branches. For example, in the first two rows ($U=0.1$, 1), we see that, for a fixed $\lambda_{\rm ext}$, a lower Δn (typically) corresponds to a *larger* relative error for HF (left column) and to a *smaller* relative error for KS (right column). Since a smaller Δn may be associated with stronger interaction, it seems that "more weakly-interacting cases", meaning $1.9\leq\Delta n\leq 2$ (in red), may be somehow more problematic than more strongly-interacting, meaning $0\leq\Delta n\leq 1$, in the DFT adiabatic connection. In the case of the MP adiabatic connection, this swap in the expected order happens only for few values in the first two panels. For example, for $U=1$ and at $|1-\lambda_{\rm ext}^{\rm HF}|\equiv 0.11$, the red curve is above the yellow one. For $U=10$, the situation becomes even more involved, as up to three different values of relative error may correspond to a given $|1-\lambda_{\rm ext}^{\rm HF}|$. While for intermediately interacting cases [$1\leq\Delta n\leq 1.9$ (in blue)], the relative error appears to be higher than for weakly interacting cases [$1.9\leq\Delta n\leq 2$ (in red)], strongly interacting cases [$0\leq\Delta n\leq 1$ (in yellow)], appear to correspond to the lowest relative error.

To conclude, it seems that $|1-\lambda_{\rm ext}|$ is an important contribution to the relative error even in the presence of a double change of curvature, however not in a straight-

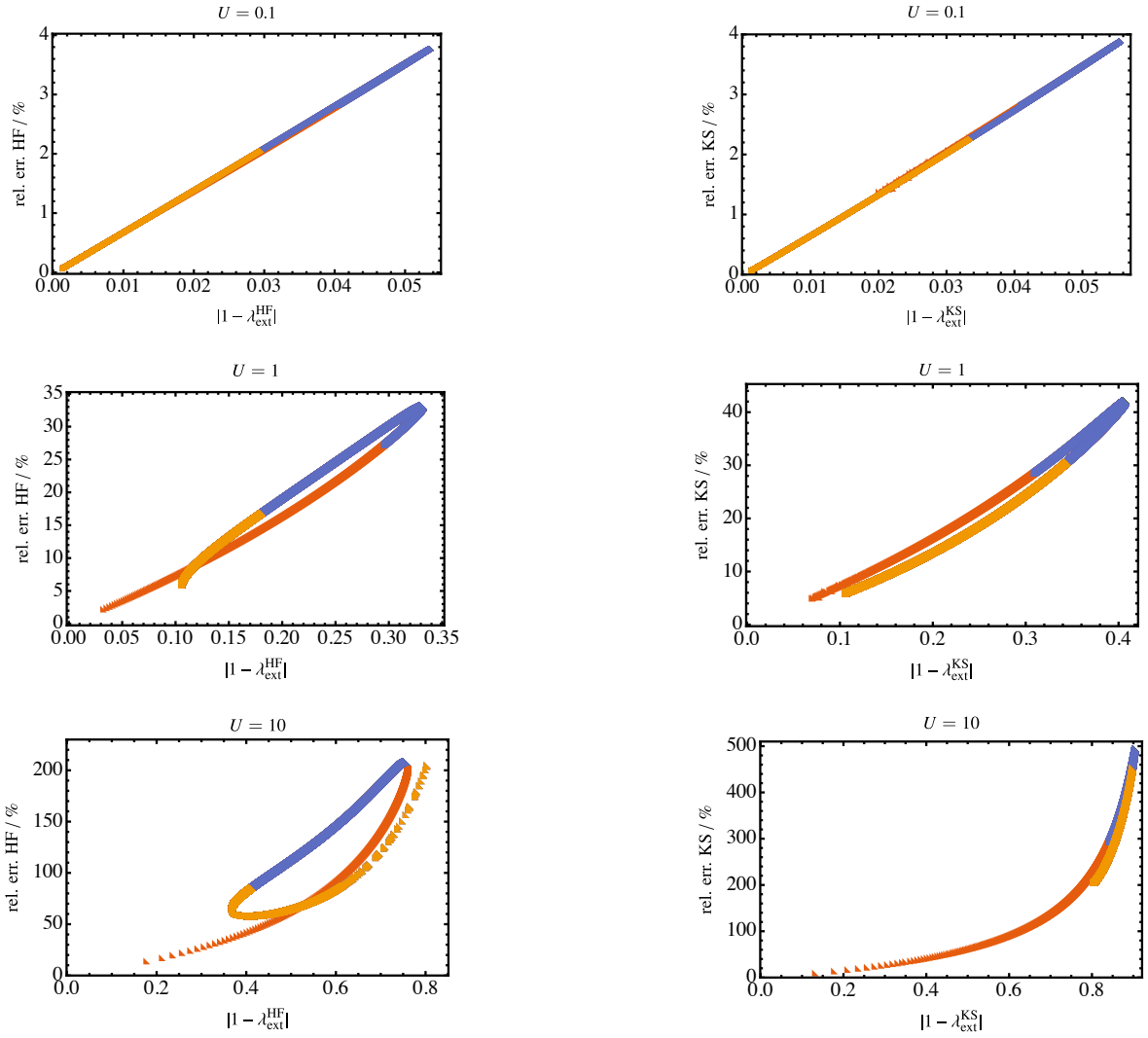

FIG. 3: Relative error in the second-order estimate of the correlation energy *vs* $|1-\lambda_{\text{ext}}|$ for different values of on-site interaction strength $U = 0.1, 1, 10$ and full domain of interacting site-occupation difference: $0 < \Delta n < 2$ (data points' spacing is 0.0001). The full domain is split into subdomains: $0 \leq \Delta n \leq 1$ (yellow), $1 \leq \Delta n \leq 1.9$ (blue), and $1.9 \leq \Delta n \leq 2$ (red). Left column concerns the Møller-Plesset adiabatic connection and E_{c}^{HF}, while right column, the DFT adiabatic connection and E_{c}^{KS}.

forward way. The question, "What relative error, y, corresponds to a $|1-\lambda_{\text{ext}}| = x$?" is ill-posed, in the sense that rather a *range* of relative error, $y \pm \Delta y$, seems to correspond to a value x. This range is different depending on whether we are considering the MP or DFT adiabatic connections and also depends on U. Unwrapping the dependence of the relative error on $|1-\lambda_{\text{ext}}|$ may be complicated, but the picture that we get from investigating these quantities in the Hubbard dimer setting seems to recommend caution when using this latter as an accuracy predictor.

On the positive side, it appears that, if $|1-\lambda_{\text{ext}}| < 0.1$, the relative error remains below 10% in all cases (regardless of U) and that, if a pair of $\{U, \Delta n\}$ makes $|1-\lambda_{\text{ext}}| < 0.1$ in one adiabatic connection, the same holds true for the other. This is because the behavior of the two adiabatic connections differs more for larger $|1-\lambda_{\text{ext}}|$. Consequently, $|1-\lambda_{\text{ext}}| < 0.1$ is the range in which this predictor is more consistent between the two adiabatic connections.

TABLE II: Mean, μ, and standard deviation, σ, for the distributions of the relative error and of $|1-\lambda_{\text{ext}}|$ accross the full site-occupation range, $0 \leq \Delta n \leq 2$, for $U = 0.1$, 1, 10 in the MP and DFT adiabatic connections ("HF" and "KS", respectively).

	$U = 0.1$		$U = 1$		$U = 10$	
	HF	KS	HF	KS	HF	KS
$\mu_{\text{rel. err.}}$	1.92	2.04	17.84	25.85	105.81	379.72
$\sigma_{\text{rel. err.}}$	2.33	2.45	20.22	28.78	115.71	392.20
$\mu_{\lvert 1-\lambda_{\text{ext}}\rvert}$	0.028	0.030	0.198	0.290	0.502	0.872
$\sigma_{\lvert 1-\lambda_{\text{ext}}\rvert}$	0.033	0.035	0.213	0.308	0.517	0.873

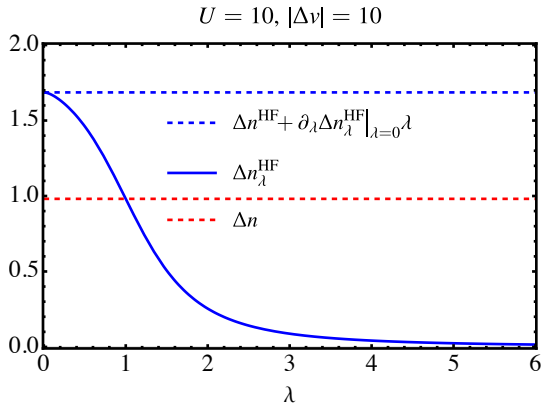

FIG. 4: Evolution of the λ-dependent site occupation, $\Delta n^{\rm HF}_\lambda$, along λ for $U = 10$ and $|\Delta v| = 10$. The tangent to the curve at $\lambda = 0$ is plotted in dashed blue, while the interacting site occupation, Δn, in dashed red.

C. The λ-dependent site occupation difference

In this section, we focus solely on the λ-dependent site occupation difference in the MP adiabatic connection, since the site-occupation difference is kept fixed in the DFT adiabatic connection by construction. Quite conveniently, in the Hubbard dimer, this quantity can be expressed analytically at any λ in the full $\{U, \Delta v\}$ parameter space (although the expression is lengthy and we eschew reporting it here). The evolution of $\Delta n^{\rm HF}_\lambda$ along λ is shown in Figure 4. Even though the plot only shows $\Delta n^{\rm HF}_\lambda$ for $U = |\Delta v| = 10$, the properties that can be observed in the figure are not specific to these values. The first thing we notice is that

$$\lim_{\lambda\to\infty} \Delta n^{\rm HF}_\lambda \sim 0 \quad \forall\, U,\, \Delta v < \infty. \tag{59}$$

Namely, for any finite Δv (or any $\Delta n^{\rm HF} < 2$), the effect of the repulsion enhanced by λ is asymptotically dominating, confining one particle on each site. Secondly, we see that the first-order derivative of the site occupation in λ is zero at $\lambda = 0$,

$$\frac{\partial \Delta n^{\rm HF}_\lambda}{\partial \lambda}\Big|_{\lambda=0} = 0, \tag{60}$$

meaning that the HF site occupation is stable under first-order variations of the coupling parameter. To see why this is the case, we use the expression of the interacting wavefunction according to perturbation theory up to first order,

$$|\Psi^{\rm HF}_\lambda\rangle \sim |\Psi^{\rm HF}_0\rangle + \lambda \sum_{i\neq 0} \frac{\langle \Psi^{\rm HF}_{0,i}|\hat{V}|\Psi^{\rm HF}_0\rangle}{E^{\rm HF}_0 - E^{\rm HF}_{0,i}} |\Psi^{\rm HF}_{0,i}\rangle, \tag{61}$$

where the perturbation operator is, following eq (36), $\hat{V} = U\sum_i \left(\hat{n}_{i\uparrow}\hat{n}_{i\downarrow} - \frac{n^{\rm HF}_i}{2}\hat{n}_i\right)$ and where the extra subscript i in $\Psi^{\rm HF}_{0,i}$ and $E^{\rm HF}_{0,i}$ indicates the spectrum of excited states and corresponding energies of the HF reference system. We omit it when indicating the GS and its energy (in other words, we write $\Psi^{\rm HF}_0$ instead of $\Psi^{\rm HF}_{0,0}$). In the Hubbard dimer, the summation is finite and exhausted with only two terms: $i = 1$ and $i = 2$, corresponding to the first and second excited states. Then, the slope of the site occupation difference around $\lambda = 0$ is given by:

$$\frac{\partial \Delta n^{\rm HF}_\lambda}{\partial \lambda}\Big|_{\lambda=0} = 2\left(\frac{\langle \Psi^{\rm HF}_{0,1}|\hat{V}|\Psi^{\rm HF}_0\rangle}{E^{\rm HF}_0 - E^{\rm HF}_{0,1}} \langle \Psi^{\rm HF}_0|\widehat{\Delta n}|\Psi^{\rm HF}_{0,1}\rangle + \frac{\langle \Psi^{\rm HF}_{0,2}|\hat{V}|\Psi^{\rm HF}_0\rangle}{E^{\rm HF}_0 - E^{\rm HF}_{0,2}} \langle \Psi^{\rm HF}_0|\widehat{\Delta n}|\Psi^{\rm HF}_{0,2}\rangle\right) \tag{62}$$

where $\widehat{\Delta n} = \hat{n}_1 - \hat{n}_0$. The first term in the summation is zero by virtue of Brillouin's theorem which makes the numerator $\langle \Psi^{\rm HF}_{0,1}|\hat{V}|\Psi^{\rm HF}_0\rangle$ vanish, as the first excited state corresponds to a singly excited determinant. On the contrary, the term $\langle \Psi^{\rm HF}_{0,2}|\hat{V}|\Psi^{\rm HF}_0\rangle$ is non-zero, but the transition dipole moment $\langle \Psi^{\rm HF}_0|\widehat{\Delta n}|\Psi^{\rm HF}_{0,2}\rangle$ is, owing to the occupation of the doubly excited state being exactly reversed compared to the ground state.

Translating the site-occupation-difference operator, $\widehat{\Delta n}$, into the density operator in real-space, $\sum_i^N \delta(\mathbf{r} - \mathbf{r}_i)$, one may thus expect that the λ-dependent density will be flat around $\lambda = 0$ also for two-electron systems in real-space whenever the transition probability $\langle \Phi^{\rm HF}|\sum_i^N \delta(\mathbf{r} - \mathbf{r}_i)|\left(\Phi^{\rm HF}\right)^{ab}_{ij}\rangle$ between any doubly-excited HF configuration and the ground HF state is negligible (or exactly zero).

IV. STRONG-INTERACTION LIMITS AND INEQUALITIES

For the Hubbard dimer, the asymptotic Hamiltonian $\hat{H}^{\rm HF}_\infty$ introduced in eq (13) reads

$$\hat{\mathcal{H}}^{\rm HF}_\infty = U\sum_i \left(\hat{n}_{i\uparrow}\hat{n}_{i\downarrow} - \frac{n^{\rm HF}_i}{2}\hat{n}_i\right) \tag{63}$$

which is diagonal in the adopted basis, the asymptotic eigenstates being simply $(100)^T, (010)^T, (001)^T$. Let us now compare the MP asymptotic Hamiltonian with the DFT one.

Although we do not know the expression of the λ-dependent external potential $\Delta v^{\lambda,\rm KS}$ at each λ in closed form, we know the large-λ behaviour of F_λ to be[44]

$$F_\lambda(\Delta n) \sim \lambda \frac{U}{2}|\Delta n| \qquad \lambda \to \infty. \tag{64}$$

Then $\lim_{\lambda\to\infty} \frac{\Delta v^{\lambda,\rm KS}}{\lambda} = \Delta v^\infty = -U\,\mathrm{sgn}(\Delta n)$, and the asymptotic Hamiltonian introduced in eq (27) reads in this case

$$\hat{\mathcal{H}}^{\rm KS}_\infty = U\sum_i \hat{n}_{i\uparrow}\hat{n}_{i\downarrow} - \frac{U}{2}\mathrm{sgn}(\Delta n)(\hat{n}_1 - \hat{n}_0). \tag{65}$$

Just as $\hat{\mathcal{H}}_\infty^{\rm HF}$, $\hat{\mathcal{H}}_\infty^{\rm KS}$ is diagonal in the adopted basis.

In Table III, we report the expectation value of the asymptotic Hamiltonian, $\hat{H}_\infty^{\rm SD}$ for the two ACs in each of the basis vectors. For the MP AC, the GS corresponds to the state where each particle is confined on each site, except for $\Delta n^{\rm HF} = \pm 2$, when the state with both particles on the site with lower external potential also contributes. So, for $|\Delta n^{\rm HF}| < 2$, the asymptotic wave function corresponds simply to $\Psi_\infty^{\rm HF} = (001)^T$ yielding $\Delta n_\infty^{\rm HF} = 0$ as already seen in Figure 4. On the contrary, for the DFT AC, the ground state is two-fold degenerate, except for $\Delta n = 0$, for which the sign of the site occupation difference is undefined and both states with two particles on one site contribute. To satisfy the density constraint, we need to make a linear combination which mixes the state with $\Delta n = 0$ with the other relevant state according to the sign of Δn. Considering, e.g., only the branch with $\Delta n > 0$, we have

$$\Psi_\infty^{\rm KS} = \begin{pmatrix} 0 \\ k \\ \sqrt{1-k^2} \end{pmatrix}, \tag{66}$$

where $k = \frac{\sqrt{\Delta n}}{\sqrt{2}}$. This picture is quite different than the usual SCE picture (in real-space) where the co-motion functions [eq (29)] enforce the density constraint. Here, this task is taken over by the coefficients of the basis vectors, which determine how the degenerate ground states are linearly combined.

Let us now consider the asymptotic AC integrands, $W_\infty^{\rm SD}$. It is quite instructive to look at how the argument used in reference 31 to prove eq (30) can be easily adapted to the Hubbard dimer case. We introduce first the bifunctional $\mathcal{W}(\Delta n, \Delta v)$ as

$$\mathcal{W}(\Delta n, \Delta v) := \min_\Psi \langle \Psi | \hat{\mathcal{U}} - \frac{\Delta v}{2}\left(\hat{n}_1 - \hat{n}_0\right) | \Psi \rangle + \frac{\Delta v}{2}\Delta n \tag{67}$$

as well as the following definitions

$$U_{\rm H}(\Delta n) := \frac{U}{2}\left(1 + \left(\frac{\Delta n}{2}\right)^2\right) \tag{68}$$

$$\Delta v_{\rm H}(\Delta n) := 2\,\frac{{\rm d}\,U_{\rm H}(\Delta n)}{{\rm d}\Delta n}. \tag{69}$$

Note that we define the Hartree energy, $U_{\rm H}$, and potential, $\Delta v_{\rm H}$ as in Ref. 45, although different definitions are possible.[44]

TABLE III: Expectation value $\langle \hat{H}_\infty^{\rm SD} \rangle$ evaluated on each of the basis vectors for SD = HF, KS.

	MP	DFT
$(100)^T$	$\frac{U}{2}\Delta n^{\rm HF}$	$U\,(1 + {\rm sgn}(\Delta n))$
$(010)^T$	$-\frac{U}{2}\Delta n^{\rm HF}$	$U\,(1 - {\rm sgn}(\Delta n))$
$(001)^T$	$-U$	0

Using the Legendre-Fenchel transform formulation of SOFT, one finds

$$\mathcal{W}(\Delta n, \Delta v^\infty(\Delta n)) = \max_{\Delta v} \mathcal{W}(\Delta n, \Delta v) \tag{70}$$

$$= \min_{\Psi \to \Delta n} \langle \Psi | \hat{\mathcal{U}} | \Psi \rangle. \tag{71}$$

On the other hand, plugging the asymptotic wave function $\Psi_\infty^{\rm KS}$ into eq (42), we have

$$W_\infty^{\rm KS}(\Delta n) = \langle \Psi_\infty^{\rm KS} | \hat{\mathcal{U}} | \Psi_\infty^{\rm KS} \rangle - U_{\rm H}(\Delta n). \tag{72}$$

Since the minimizer in eq (71) is precisely $\Psi_\infty^{\rm KS}$, we have

$$\left(W_\infty^{\rm KS} + U_{\rm H}\right)(\Delta n) = \max_{\Delta v} \mathcal{W}(\Delta n, \Delta v). \tag{73}$$

In the MP strong-interaction case, we cannot make use of any convex analysis tool. However, substituting the asymptotic wave function $\Psi_\infty^{\rm HF}$ into definition (39) for general λ and using Eqs. (67), (68) and (69), one obtains

$$\left(W_\infty^{\rm HF} + U_{\rm H}\right)\left(\Delta n^{\rm HF}\right) = \mathcal{W}(\Delta n^{\rm HF}, \Delta v_{\rm H}(\Delta n^{\rm HF})) \tag{74}$$

Choosing now $\Delta n \equiv \Delta n^{\rm HF}$ and comparing Eqs. (73) and (74) leads to

$$W_\infty^{\rm HF}(\Delta n^{\rm HF}) \leq W_\infty^{\rm KS}(\Delta n)\Big|_{\Delta n \equiv \Delta n^{\rm HF}} \tag{75}$$

which is the Hubbard dimer analogue of eq (30).

In practice, we can also work out the explicit expressions, which read

$$W_\infty^{\rm HF}(\Delta n^{\rm HF}) = \frac{U}{2}\left(\left(\frac{\Delta n^{\rm HF}}{2}\right)^2 - 1\right), \tag{76}$$

and

$$W_\infty^{\rm KS}(\Delta n) = -\frac{U}{2}\left(1 - \left|\frac{\Delta n}{2}\right|\right)^2 \tag{77}$$

This latter expression is in agreement with eq (56) of reference 44 (as in the *corrigendum*[57]) for $E_c^{\rm KS}$ in the $U \to \infty$ limit. This limit corresponds to the situation where the indirect interaction energy (the on-site repulsion minus the mean field term) becomes dominant and, indeed, we have $E_c^{\rm KS} \sim U_c^{\rm KS} \sim W_\infty^{\rm KS}$ as $U \to \infty$, while $T_c^{\rm KS}$ is subleading. In the HF case, we do have

$$E_c^{\rm HF} \sim W_\infty^{\rm HF} \qquad \text{for} \quad U \to \infty, \tag{78}$$

with $T_c^{\rm HF}$ similarly subleading; however in this case the extra term coming from the external potential remains non-negligible at large U and contributes to $W_\infty^{\rm HF}$. Introducing the leading-order terms in the large-λ expansions of the individual components [eq (53)],

$$\lim_{\lambda\to\infty} U_{c,\lambda}^{\rm HF} = U_{c,\infty}^{\rm HF}\,\lambda + o(\lambda) \tag{79a}$$

$$\lim_{\lambda\to\infty} V_{c,\lambda}^{\rm HF} = V_{c,\infty}^{\rm HF}\,\lambda + o(\lambda), \tag{79b}$$

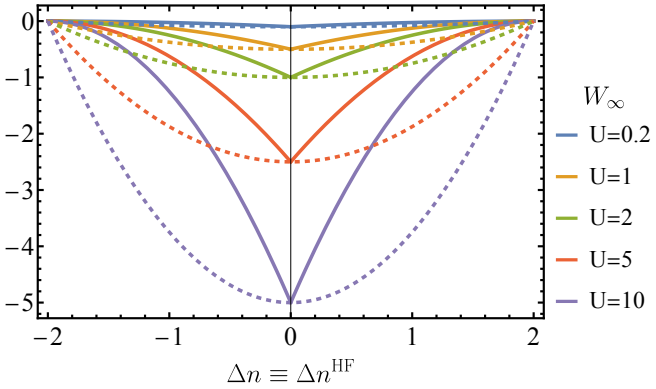

FIG. 5: Strong-interaction limit as a function of the occupation, $W_\infty(\Delta n)$, of the MP (dashed) and of the DFT (solid) adiabatic connections.

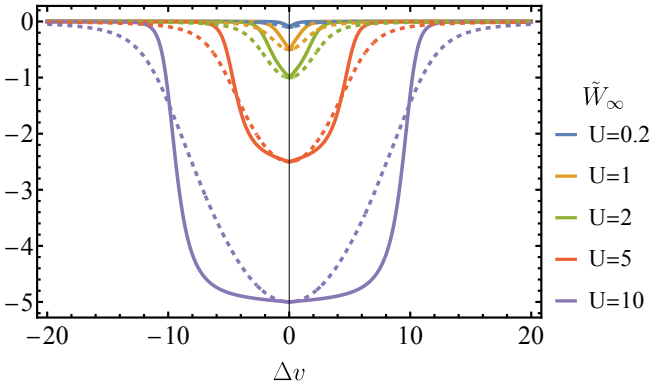

FIG. 6: Strong-interaction limit as a function of the external potential, $\tilde{W}_\infty(\Delta v)$ of the MP (dashed) and of the DFT (solid) adiabatic connections.

where $U^{\rm HF}_{c,\infty} = -U_{\rm H}(\Delta n^{\rm HF})$ and $V^{\rm HF}_{c,\infty} = -U$, then

$$W^{\rm HF}_\infty = U^{\rm HF}_{c,\infty} + V^{\rm HF}_{c,\infty}. \tag{80}$$

The quantities $W^{\rm KS}_\infty$ and $W^{\rm HF}_\infty$ are plotted in fig 6 for the same site-occupation difference; from which the inequality (75) nicely stands out (the dashed line which corresponds to $W^{\rm HF}_\infty$ is always below the thick one except at $\Delta n = 0$). However, considering that both the interacting and the HF site-occupation differences are known analytically as functions of the external potential difference, Δv, it becomes interesting to look at how the two asymptotic AC integrands relate to one another for the same interacting Hamiltonian (same $\{U, \Delta v\}$ pair), plotted in fig 6. From the figure, we can see that there is actually a significant range of Δv, at fixed U, for which the DFT asymptotic AC integrand is actually lower than the MP one. This may come as a surprise, since, in fig 1, no such cases are shown, but this is only because we chose to plot examples from the three different regimes $U/|\Delta v| = 0.1, 1, 10$. However, choosing, e.g., $U = 10$ and $\Delta v = 5$, the DFT asymptotic AC integrand is lower than the MP (compare fig 6). Indeed, in fig 7 where both AC integrands are plotted along λ for these parameters, we observe that the MP AC integrand remains always *above* the DFT one.

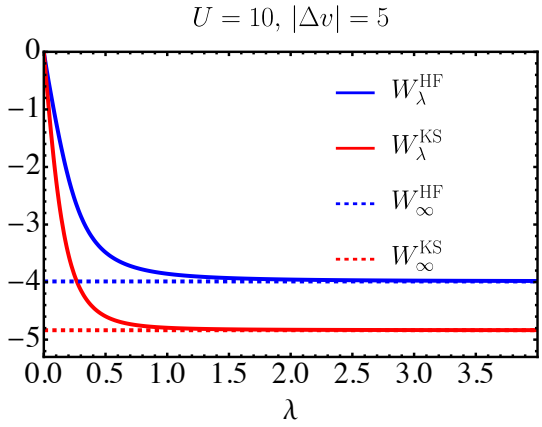

FIG. 7: Example of U and Δv parameters for which $W^{\rm KS}_\infty < W^{\rm HF}_\infty$.

V. CONCLUSIONS AND PERSPECTIVES

In this work, we have calculated the Møller-Plesset (MP) and the density-fixed (DFT) adiabatic connection for the asymmetric Hubbard dimer. The Hamiltonian of this model is fully determined by only two parameters, e.g., interaction strength and external potential (or interaction strength and site occupation), allowing one to investigate the two adiabatic connections systematically at different correlation regimes. The main result we report is that, while the DFT adiabatic connection integrand appears to be convex for any value of the parameters $\{U, \Delta v\}$ (in line with expectations), the MP integrand shows a double change of curvature for a continuous range of Δv, at any given $U > 0$. Since the Hubbard dimer is often considered as a prototype for a stretched diatomic molecule, our finding might signal the presence of such previously unexpected behaviour also in molecular systems. We have argued that the external potential contribution to $E^{\rm HF}_c$ ($V^{\rm HF}_c$), which is absent in $E^{\rm KS}_c$, may be responsible for the extra flexibility of the MP adiabatic connection over the DFT one, and we have derived an inequality between the MP2 and GL2 correlation energies [eq (52)]. We have calculated the accuracy predictor based on $\lambda_{\rm ext}$ of eq (58) in the complete site-occupation range ($0 \leq \Delta n < 2$) and contrasted it with the relative error corresponding to the MP2/GL2 correlation energies (Figure 3). For the MP adiabatic connection, we have shown that the derivative of the site-occupation with respect to λ is zero around the HF density, for any $\{U, \Delta v\}$ pair (section III C).

Finally, we have characterised the strong-interaction limit in both adiabatic connections for our model. While the asymptotic MP wave function, $\Psi^{\rm HF}_\infty$, is simply the symmetry-adapted state with one particle on each site,

the DFT asymptotic state must mix in the state with two-particles on the same site as well, with a coefficient determined by the density constraint [eq (66)]. The inequality relating the asymptotic adiabatic connection integrands, W_∞^{HF} and W_∞^{KS}, that holds for a given density in real-space [eq (30)] has been translated in the lattice setting [eq (75)], and the two quantities have been compared also for a given external potential (see Figure 6).

As the double change of curvature is an important element to keep in mind in the use of adiabatic connection interpolation methods, a possible next step could be to calculate the MP adiabatic connection for the H_2 molecule at large internuclear distances to verify whether this feature is present also in actual molecular systems (other models, such as the Moshinsky atom[58] may be used). Constructing the MP adiabatic connection integrand for the UHF reference state for the asymmetric Hubbard dimer could also shed some light on the origin of this feature.

Another extension of this work, in the spirit of developing functional approximations that use the HF density as reference, may be to construct a λ-dependent local density approximation from Quantum Monte Carlo data for the uniform electron gas along the MP adiabatic connection. Such data could also reveal whether the double change of curvature and/or the behaviour of the λ-dependent density being flat around the HF density [eq (60)] are encountered in the uniform electron gas.

[1] Pernal, K. Electron correlation from the adiabatic connection for multireference wave functions. *Phys. Rev. Lett.* **2018**, *120*, 013001.

[2] Pernal, K. Correlation energy from random phase approximations: A reduced density matrices perspective. *Int. J. Quantum Chem.* **2018**, *118*, e25462.

[3] Pastorczak, E.; Pernal, K. Correlation energy from the adiabatic connection formalism for complete active space wave functions. *J. Chem. Theory Comput.* **2018**, *14*, 3493–3503.

[4] Pernal, K. Exact and approximate adiabatic connection formulae for the correlation energy in multireference ground and excited states. *J. Chem. Phys.* **2018**, *149*, 204101.

[5] Pastorczak, E.; Pernal, K. Electronic excited states from the adiabatic-connection formalism with complete active space wave functions. *J. Phys. Chem. Lett.* **2018**, *9*, 5534–5538.

[6] Pastorczak, E.; Hapka, M.; Veis, L.; Pernal, K. Capturing the dynamic correlation for arbitrary spin-symmetry CASSCF reference with adiabatic connection approaches: Insights into the electronic structure of the tetramethyleneethane diradical. *J. Phys. Chem. Lett.* **2019**, *10*, 4668–4674.

[7] Drwal, D.; Pastorczak, E.; Pernal, K. Excited states in the adiabatic connection fluctuation-dissipation theory: Recovering missing correlation energy from the negative part of the density response spectrum. *J. Chem. Phys.* **2021**, *154*, 164102.

[8] Beran, P.; Matoušek, M.; Hapka, M.; Pernal, K.; Veis, L. Density matrix renormalization group with dynamical correlation via adiabatic connection. *J. Chem. Theory Comput.* **2021**, *17*, 7575–7585.

[9] Drwal, D.; Beran, P.; Hapka, M.; Modrzejewski, M.; Sokół, A.; Veis, L.; Pernal, K. Efficient Adiabatic Connection Approach for Strongly Correlated Systems: Application to Singlet–Triplet Gaps of Biradicals. *J. Phys. Chem. Lett.* **2022**, *13*, 4570–4578.

[10] Matoušek, M.; Hapka, M.; Veis, L.; Pernal, K. Toward more accurate adiabatic connection approach for multireference wavefunctions. *J. Chem. Phys.* **2023**, *158*, 054105.

[11] Harris, J.; Jones, R. The surface energy of a bounded electron gas. *J. Physical. F* **1974**, *4*, 1170.

[12] Gunnarsson, O.; Lundqvist, B. I. Exchange and correlation in atoms, molecules, and solids by the spin-density-functional formalism. *Phys. Rev. B* **1976**, *13*, 4274–4298.

[13] Langreth, D. C.; Perdew, J. P. The exchange-correlation energy of a metallic surface. *Solid. State Commun.* **1975**, *17*, 1425–1429.

[14] Kohn, W.; Sham, L. J. Self-Consistent Equations Including Exchange and Correlation Effects. *Phys. Rev.* **1965**, *140*, A1133–A1138.

[15] Becke, A. D. A new mixing of Hartree–Fock and local density-functional theories. *J. Chem. Phys.* **1993**, *98*, 1372.

[16] Perdew, J. P.; Ernzerhof, M.; Burke, K. Rationale for mixing exact exchange with density functional approximations. *J. Chem. Phys.* **1996**, *105*, 9982–9985.

[17] Sharkas, K.; Toulouse, J.; Savin, A. Double-hybrid density- functional theory made rigorous. *J. Chem. Phys.* **2011**, *134*, 064113.

[18] Furche, F. Molecular tests of the random phase approximation to the exchange-correlation energy functional. *Phys. Rev. B* **2001**, *64*, 195120.

[19] Ernzerhof, M. Construction of the adiabatic connection. *Chem. Phys. Lett.* **1996**, *263*, 499.

[20] Seidl, M.; Perdew, J. P.; Levy, M. Strictly correlated electrons in density-functional theory. *Phys. Rev. A* **1999**, *59*, 51–54.

[21] Seidl, M.; Perdew, J. P.; Kurth, S. Simulation of All-Order Density-Functional Perturbation Theory, Using the Second Order and the Strong-Correlation Limit. *Phys. Rev. Lett.* **2000**, *84*, 5070–5073.

[22] Liu, Z.-F.; Burke, K. Adiabatic connection in the low-density limit. *Phys. Rev. A* **2009**, *79*, 064503.

[23] Gori-Giorgi, P.; Vignale, G.; Seidl, M. Electronic Zero-Point Oscillations in the Strong-Interaction Limit of Density Functional Theory. *J. Chem. Theory Comput.* **2009**, *5*, 743–753.

[24] Constantin, L. A. Correlation energy functionals from adiabatic connection formalism. *Phys. Rev. B* **2019**, *99*, 085117.

[25] Vuckovic, S.; Gori-Giorgi, P.; Della Sala, F.; Fabiano, E. Restoring size consistency of approximate functionals constructed from the adiabatic connection. *J. Phys. Chem. Lett.* **2018**, *9*, 3137–3142.

[26] Fabiano, E.; Gori-Giorgi, P.; Seidl, M.; Della Sala, F. Interaction-Strength Interpolation Method for Main-Group Chemistry: Benchmarking, Limitations, and Perspectives. *J. Chem. Theory. Comput.* **2016**, *12*, 4885–4896.

[27] Vuckovic, S.; Fabiano, E.; Gori-Giorgi, P.; Burke, K. MAP: an MP2 accuracy predictor for weak interactions from adiabatic connection theory. *J. Chem. Theory Comput.* **2020**, *16*, 4141–4149.

[28] Daas, T. J.; Fabiano, E.; Della Sala, F.; Gori-Giorgi, P.; Vuckovic, S. Noncovalent interactions from models for the møller–plesset adiabatic connection. *J. Phys. Chem. Lett.* **2021**, *12*, 4867–4875.

[29] Fabiano, E.; Śmiga, S.; Giarrusso, S.; Daas, T. J.; Della Sala, F.; Grabowski, I.; Gori-Giorgi, P. Investigation of the exchange-correlation potentials of functionals based on the adiabatic connection interpolation. *J. Chem. Theory Comput.* **2019**, *15*, 1006–1015.

[30] Śmiga, S.; Della Sala, F.; Gori-Giorgi, P.; Fabiano, E. Self-consistent Kohn-Sham calculations with adiabatic connection models. *arXiv preprint arXiv:2202.11531* **2022**,

[31] Seidl, M.; Giarrusso, S.; Vuckovic, S.; Fabiano, E.; Gori-Giorgi, P. Communication: Strong-interaction limit of an adiabatic connection in Hartree-Fock theory. *J. Chem. Phys.* **2018**, *149*, 241101.

[32] Daas, T. J.; Kooi, D. P.; Grooteman, A. J.; Seidl, M.; Gori-Giorgi, P. Gradient expansions for the large-coupling strength limit of the møller–plesset adiabatic connection. *J. Chem. Theory Comput.* **2022**, *18*, 1584–1594.

[33] Vuckovic, S.; Gerolin, A.; Daas, T. J.; Bahmann, H.; Friesecke, G.; Gori-Giorgi, P. Density functionals based on the mathematical structure of the strong-interaction limit of DFT. *Wiley Interdiscip. Rev. Comput. Mol. Sci.* **2022**, e1634.

[34] Daas, T. J.; Grossi, J.; Vuckovic, S.; Musslimani, Z. H.; Kooi, D. P.; Seidl, M.; Giesbertz, K. J.; Gori-Giorgi, P. Large coupling-strength

expansion of the Møller–Plesset adiabatic connection: From paradigmatic cases to variational expressions for the leading terms. *J. Chem. Phys.* **2020**, *153*, 214112.

[35]Langreth, D. C. New theoretical support for density-functional theory as commonly applied. *Phys. Rev. Lett.* **1984**, *52*, 2317.

[36]Levy, M. Universal variational functionals of electron densities, first-order density matrices, and natural spin-orbitals and solution of the v-representability problem. *Proc. Natl. Acad. Sci.* **1979**, *76*, 6062–6065.

[37]Görling, A.; Levy, M. Correlation-energy functional and its high-density limit obtained from a coupling-constant perturbation expansion. *Phys. Rev. B* **1993**, *47*, 13105.

[38]Görling, A.; Levy, M. Exact Kohn-Sham scheme based on perturbation theory. *Phys. Rev. A* **1994**, *50*, 196.

[39]Seidl, M. Strong-interaction limit of density-functional theory. *Phys. Rev. A* **1999**, *60*, 4387–4395.

[40]Seidl, M.; Gori-Giorgi, P.; Savin, A. Strictly correlated electrons in density-functional theory: A general formulation with applications to spherical densities. *Phys. Rev. A* **2007**, *75*, 042511/12.

[41]Giarrusso, S.; Vuckovic, S.; Gori-Giorgi, P. Response potential in the strong-interaction limit of DFT: Analysis and comparison with the coupling-constant average. *J. Chem. Theory Comput.* **2018**, *14*, 4151–4167.

[42]Lewin, M. Semi-classical limit of the Levy–Lieb functional in density functional theory. *C. R. Math.* **2018**, *356*, 449–455.

[43]Lieb, E. H. Density Functionals for CouIomb Systems. *Int. J. Quantum. Chem.* **1983**, *24*, 243–277.

[44]Carrascal, D.; Ferrer, J.; Smith, J. C.; Burke, K. The Hubbard dimer: a density functional case study of a many-body problem. *J. Phys. Condens.* **2015**, *27*, 393001.

[45]Giarrusso, S.; Pribram-Jones, A. Comparing correlation components and approximations in Hartree–Fock and Kohn–Sham theories via an analytical test case study. *J. Chem. Phys.* **2022**, *157*, 054102.

[46]van Leeuwen, R. Kohn-Sham potentials in density functional theory. Academisch proefschrift, Vrije Universiteit van Amsterdam, 1994.

[47]Helgaker, T.; Teale, A. M. *The Physics and Mathematics of Elliott Lieb*; EMS Press, 2022; pp 527–559.

[48]Colonna, F.; Savin, A. Correlation energies for some two-and four-electron systems along the adiabatic connection in density functional theory. *J. Chem. Phys.* **1999**, *110*, 2828–2835.

[49]Savin, A.; Colonna, F.; Pollet, R. Adiabatic connection approach to density functional theory of electronic systems. *Int. J. Quantum Chem.* **2003**, *93*, 166–190.

[50]Wu, Q.; Yang, W. A direct optimization method for calculating density functionals and exchange–correlation potentials from electron densities. *J. Chem. Phys.* **2003**, *118*, 2498–2509.

[51]Teale, A. M.; Coriani, S.; Helgaker, T. The calculation of adiabatic-connection curves from full configuration-interaction densities: Two-electron systems. *J. Chem. Phys.* **2009**, *130*, 104111.

[52]Teale, A. M.; Coriani, S.; Helgaker, T. Accurate calculation and modeling of the adiabatic connection in density functional theory. *J. Chem. Phys.* **2010**, *132*, 164115.

[53]Strømsheim, M. D.; Kumar, N.; Coriani, S.; Sagvolden, E.; Teale, A. M.; Helgaker, T. Dispersion interactions in density-functional theory: An adiabatic-connection analysis. *J. Chem. Phys.* **2011**, *135*, 194109.

[54]Vuckovic, S.; Irons, T. J.; Savin, A.; Teale, A. M.; Gori-Giorgi, P. Exchange–correlation functionals via local interpolation along the adiabatic connection. *J. Chem. Theory Comput.* **2016**, *12*, 2598–2610.

[55]Vuckovic, S.; Irons, T. J.; Wagner, L. O.; Teale, A. M.; Gori-Giorgi, P. Interpolated energy densities, correlation indicators and lower bounds from approximations to the strong coupling limit of DFT. *Phys. Chem. Chem. Phys.* **2017**, *19*, 6169–6183.

[56]Giarrusso, S.; Gori-Giorgi, P.; Della Sala, F.; Fabiano, E. Assessment of interaction-strength interpolation formulas for gold and silver clusters. *J. Chem. Phys.* **2018**, *148*, 134106.

[57]Carrascal, D.; Ferrer, J.; Smith, J.; Burke, K. Corrigendum: The Hubbard dimer: a density functional case study of a many-body problem (2015 J. Phys.: Condens. Matter 27 393001). *J. Phys. Condens.* **2016**, *29*.

[58]Moshinsky, M. How good is the Hartree-Fock approximation. *Am. J. Phys.* **1968**, *36*, 52–53.